

Influence of the coupled-dipoles on photosynthetic performance in a photosynthetic quantum heat engine

Ling-Fang Li(李玲芳) and Shun-Cai Zhao(赵顺才)†

Citation: Chin. Phys. B, 2021, 30 (**4**): 044215. DOI: 10.1088/1674-1056/abdea6
Journal homepage: http://cpb.iphy.ac.cn; http://iopscience.iop.org/cpb

What follows is a list of articles you may be interested in

Sensitivity enhancement of micro-optical gyro with photonic crystal

Liu Yang(杨柳), Shuhua Zhao(赵舒华), Jingtong Geng(耿靖童), Bing Xue(薛冰), and Yonggang Zhang(张勇刚)
Chin. Phys. B, 2021, 30 (**4**): 044208. DOI: 10.1088/1674-1056/abe3f3

Nonlinear spectroscopy of three-photon excitation of cesium Rydberg atoms in vapor cell

Jiabei Fan(樊佳蓓), Yunhui He(何云辉), Yuechun Jiao(焦月春), Liping Hao(郝丽萍), Jianming Zhao(赵建明), and Suotang Jia(贾锁堂)
Chin. Phys. B, 2021, 30 (**3**): 034207. DOI: 10.1088/1674-1056/abca25

An ultrafast and low-power slow light tuning mechanism for compact aperture-coupled disk resonators

Bo-Yun Wang(王波云), Yue-Hong Zhu(朱月红), Jing Zhang(张静), Qing-Dong Zeng(曾庆栋), Jun Du(杜君), Tao Wang(王涛), Hua-Qing Yu(余华清)
Chin. Phys. B, 2020, 29 (**8**): 084211. DOI: 10.1088/1674-1056/ab9df1

Inhibiting radiative recombination rate to enhance quantum yields in a quantum photocell

Jing-Yi Chen(陈镜伊), Shun-Cai Zhao(赵顺才)
Chin. Phys. B, 2020, 29 (**6**): 064207. DOI: 10.1088/1674-1056/ab836f

Electromagnetically induced transparency and electromagnetically induced absorption in Y-type system

Kalan Mal, Khairul Islam, Suman Mondal, Dipankar Bhattacharyya, Amitava Bandyopadhyay
Chin. Phys. B, 2020, 29 (**5**): 054211. DOI: 10.1088/1674-1056/ab7ea0

Influence of the coupled-dipoles on photosynthetic performance in a photosynthetic quantum heat engine*

Ling-Fang Li(李玲芳) and Shun-Cai Zhao(赵顺才)†

Department of Physics, Kunming University of Science and Technology, Kunming 650500, *China*

(Received 3 December 2020; revised manuscript received 17 January 2021; accepted manuscript online 22 January 2021)

Recent evidence suggests that the multiple charge-separation pathways can contribute to photosynthetic performance. In this work, the influence of coupled-dipoles on photosynthetic performance was investigated in a two-charge separation pathways quantum heat engine (QHE) model. And the population dynamics of the two coupled sites, *j*–*V* characteristics, and power involving this photosynthetic QHE model were evaluated for the photosynthetic performance. The results illustrate that the photosynthetic performance can be greatly enhanced but quantum interference is deactivated by the coupled-dipoles between the two-charge separation pathways. However, the photosynthetic performance can also be promoted by the deactivated quantum interference owing to the coupled-dipoles. It is a novel role of the coupled-dipoles in the energy transport process of biological photosynthetic, and some artificial strategies may be motivated by this photosynthetic QHE model in the future.

Keywords: photosynthetic performance, coupled-dipole, photosynthetic heat engine

PACS: 42.50.Gy, 42.50.−p, 32.80.Qk **DOI:** 10.1088/1674-1056/abdea6

1. Introduction

Charge separation is an essential process in the conversion of solar energy into chemical energy in photosynthesis.[1] After absorption of a photon which creates an electronically excited state in a pigment molecule, the excited state is transformed into a short-lived charge-separated state until it arrives at a reaction center (RC)[2–6] in the pigment-protein complex and results in a stable charge-separated state, which ultimately powers the photosynthetic organism.[7] The photon-to-charge conversion efficiency in the above process is considered close to 100% under certain conditions.[8–11] This eye-catching result sparks the researchers to explore its physics behind the energy conversion within photosynthesis.[12,13] People firmly believe that understanding its underlying mechanism involving photosynthesis can help us design novel artificial nanodevices for efficient quantum transport and some optimized solar cells.[14–18] Recently, some theoretical models[19–21] show that quantum mechanical behavior contributes to the high efficiency of biological processes.

Simulating the photosynthetic RC as a biological QHE, Dorfman *et al.*[22] suggested that photocurrent can be improved by noise-induced coherence in the photosynthetic RC. Creatore *et al.*[23] proposed a model for photosynthetic RC in which quantum mechanical effects were investigated. The results show that photo-to-charge conversion can be boosted via quantum interference caused by dipole–dipole interactions[24] between molecular excited states. And compared with classical photocell, this effect can increase the current and power output by 35%. In a multiple charge-separation pathways scheme,[25] the results demonstrated that a multi-pathway biological QHE was a better choice for the charge separation, improving the quantum current and power yield. Recently, long-lived quantum coherence in the pigment-protein complexes was observed and extensively investigated in some experiments.[1,26–29]

Although electron transfer in the photosynthetic RC has been thoroughly investigated in one or several charge-separation pathways, and it is believed that two main pathways make a significant contribution to the current and power in the photosynthetic process.[30] However, works on the influence of the coupled-dipoles between two different charge separation pathways are rarely found. Therefore, we consider the coupled-dipoles between two different charge separation pathways involving the photosynthetic performance in a double-pathway[31] photosynthetic QHE model, which is different from the work that discussed the system–bath coupling effect on the exciton-transfer processes in the photosystem II reaction center via the polaron master-equation approach[32] in a QHE model. We no longer care about the impact of multi-charge-separation pathways,[25,30] but turn our attention to the impact of the coupled-dipoles on the photosynthetic performance. We are focusing on whether the coupled-dipole is more beneficial to enhance the photosynthetic performances in this two-pathways biological QHE model, which can be used to mimic the process in the RC of the light-harvesting complex phycocyanin-645 (PC645) with a pair of strongly coupled sites (called DBV C and DBV D).[12,33]

*Project supported by the National Natural Science Foundation of China (Grant Nos. 62065009 and 61565008) and the General Program of Yunnan Applied Basic Research Project, China (Grant No. 2016FB009).

†Corresponding author. E-mail: zhaosc@kmust.edu.cn

© 2021 Chinese Physical Society and IOP Publishing Ltd

2. Model and equation

Here, we investigate the influence of the coupled-dipoles in a two-pathway QHE model illustrated in Fig. 1, which is abstracted from the photosystem II reaction center (PSII-RC) consisting of six core pigment molecules. The typical PSII-RC found in purple bacteria and oxygen-evolving organisms (cyanobacteria, algae, and higher plants) contains six pigment molecules coupled by the dipole-dipole interactions,[34–36] and the six pigments are arranged in two symmetric branches of the protein matrix in the center of the complex. Four chlorophylls of them (special pair PD_1, PD_2 and accessory $ChlD_1$, $ChlD_2$) and two pheophytins ($PheD_1$, $PheD_2$) are parallel distributed in these two branches of the protein matrix. The pair of chlorophylls, PD_1, PD_2 located at the center of the PSII RC act as the primary electron donors, forming two exciton states denoted as $|e_{1,2}\rangle$ in Fig. 1. Two pheophytin pigments, $PheD_1$ and $PheD_2$ couple to the rest of the molecules, and $PheD_1$ plays the part of electron acceptor[34–36] in the charge-separation process of the PSII RC.

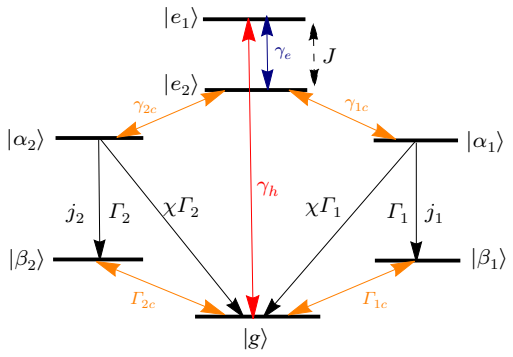


Fig. 1. Energy-level framework of photosynthetic QHE for the photosynthetic RC with two load-transitions $|\alpha_i\rangle \to |\beta_i\rangle_{i=1,2}$. The electronic transition from the ground state $|g\rangle$ to two coupled dipoles $|e_1\rangle$,$|e_2\rangle$ is induced by the high temperature photon bath. The low temperature phonon bath drives charge transfer from the level $|e_2\rangle \to |\alpha_i\rangle_{i=1,2}$, and $|\beta_i\rangle_{i=1,2} \to |g\rangle$ with termination of the electronic circulation.

As shown in Fig. 1, after the absorption of a solar photon, the excited electron is promoted from $|g\rangle$ to $|e_2\rangle$ and/or $|e_1\rangle$ with the transition rate γ_h, and the excited electron may transit to $|e_1\rangle$ state at the rate γ_e. Then the excited electron is transferred to the acceptors by the emission of a phonon via two pathways: $|e_1\rangle$ ($|e_2\rangle$)$\to$ $|\alpha_1\rangle$ and $|e_1\rangle$ ($|e_2\rangle$)$\to$ $|\alpha_2\rangle$ at the emissions rates $\gamma_{ic(i=1,2)}$ with $|\alpha_1\rangle$ and $|\alpha_2\rangle$ being the ion-pair states in these two pathways. Furthermore, the positive and negative charges are spatially separated by releasing the excited electron to the plastoquinone molecule and leaving a hole in the dimer. Eventually, the electron is transferred to the final electron acceptor $PheD_1$, from which the electron is released to perform work[23] with a rate $|\Gamma_i\rangle_{(i=1,2)}$, denoted by $|\alpha_1\rangle \to |\beta_1\rangle$ (path 1) and $|\alpha_2\rangle \to |\beta_2\rangle$ (path 2) in Fig. 1. Finally, the electron returns to the primary electron donor via $|\beta_1\rangle$ ($|\beta_2\rangle$) $\to |g\rangle$. Similarly, the acceptor-to-donor charge recombination for two pathways, described by $|\alpha_1\rangle$ ($|\alpha_2\rangle$) $\to$ $|g\rangle$ with rate $\chi\Gamma_{i=1,2}$, brings the system back to the ground state $|g\rangle$ but does not produce current, where χ is a dimensionless fraction[37] describing the radiative recombination rate of the two pathways. From the physical perspective, we assume the load transition is unidirectional, which means that only the photosynthetic heat engine can transfer energy to the load, not the other way around. Therefore, the total current is given by $j = e\sum_{i=1}^{2}\Gamma_i\rho_{\alpha_i\alpha_i}$, with e being the elementary electron charge.

To clarify the influence caused by the coupled-dipoles, we will evaluate the photosynthetic performances via the current and power involving this photosynthetic QHE numerically. Therefore, we considered the dipole-dipole coupling depicted by two excited states $|e_{1/2}\rangle = \frac{1}{\sqrt{2}}(|D_1\rangle \pm |D_2\rangle)$[38] between the two different charge separation pathways with their eigenenergies $E_{e1/e2} = E_{D_1/D_2} \pm J$, where J depicts the coupling robustness illustrated in Fig. 1. The state $|D_{i=1,2}\rangle$ describes chlorophylls PD_i, the electron donors. With this knowledge, the Hamiltonian of this QHE model consists of three parts: the electronic Hamiltonian is read as

$$\begin{aligned}\hat{H}_e =& E_g|g\rangle\langle g| + \sum_{i=1}^{2}(E_{\alpha_i}|\alpha_i\rangle\langle\alpha_i| + E_{\beta_i}|\beta_i\rangle\langle\beta_i| + E_{D_i}|D_i\rangle\langle D_i|) \\ &+ J(|D_1\rangle\langle D_2| + |D_2\rangle\langle D_1|). \end{aligned} \tag{1}$$

A full microscopic mode Hamiltonian is given as follows:

$$\hat{H}_0 = \sum_k \hbar\omega_k \hat{a}_k^\dagger \hat{a}_k. \tag{2}$$

Considering the above modes and ambient reservoirs linearly coupled to the electrical system,[37,39] the interaction Hamiltonian can be written in rotating-wave approximation as follows:

$$\hat{H}_v = \hat{V}_H + \hat{V}_{1c} + \hat{V}_{2c} + \hat{V}_{3c}, \tag{3}$$

where the items in the above expression are given in the following forms:

$$\begin{aligned}\hat{V}_H &= \sum_k \hbar(\varepsilon_{hk}\hat{\sigma}_{g1}\otimes\hat{a}_{hk}^\dagger + \varepsilon_{hk}^*\hat{\sigma}_{g1}^\dagger\otimes\hat{a}_{hk}), \\ \hat{V}_{1c} &= \sum_{i=1}^{2}\sum_k \hbar(\varepsilon_{1ck}\hat{\sigma}_{i2}\otimes\hat{a}_{1ck}^\dagger + \varepsilon_{1ck}^*\hat{\sigma}_{i2}^\dagger\otimes\hat{a}_{1ck}), \\ \hat{V}_{2c} &= \sum_{i=1}^{2}\sum_k \hbar(\varepsilon_{2ck}\hat{\sigma}_{gi}\otimes\hat{a}_{2ck}^\dagger + \varepsilon_{2ck}^*\hat{\sigma}_{gi}^\dagger\otimes\hat{a}_{2ck}), \\ \hat{V}_{3c} &= \sum_k \hbar(\varepsilon_{3ck}\hat{\sigma}_{21}\otimes\hat{a}_{3ck}^\dagger + \varepsilon_{3ck}^*\hat{\sigma}_{21}^\dagger\otimes\hat{a}_{3ck}), \end{aligned} \tag{4}$$

where ε_{ik} $(i = h, 1c, 2c, 3c)$ is the corresponding couple strength of pigment i to the k-th mode of the reservoir, $\hat{a}_{ik}^\dagger(\hat{a}_{ik})$ $(i = h, 1c, 2c, 3c)$ are the creation(annihilation) operator of k-th reservoir mode, the system operators are defined as $\hat{\sigma}_{g1} = |g\rangle\langle e_1|, \hat{\sigma}_{i2} = |\alpha_i\rangle\langle e_2|$ $(i = 1, 2), \hat{\sigma}_{gi} = |g\rangle\langle\beta_i|_{(i=1,2)}$, and $\hat{\sigma}_{21} = |e_2\rangle\langle e_1|$.

The total system Hamiltonian, $\hat{H}_T = \hat{H}_e + \hat{H}_0 + \hat{H}_v$, where the electronic Hamiltonian $\hat{H}_e$ describes the unitary evolution of the electron transfer via the Lindblad-type master equation

$$\frac{\mathrm{d}\hat{\rho}}{\mathrm{d}t} = -\mathrm{i}[\hat{H}_e, \hat{\rho}] + \mathcal{L}_H\hat{\rho} + \mathcal{L}_{1c}\hat{\rho} + \mathcal{L}_{2c}\hat{\rho} + \mathcal{L}_{3c}\hat{\rho} + \mathcal{L}_\Gamma\hat{\rho} + \mathcal{L}_{\lambda\Gamma}\hat{\rho}. \tag{5}$$

The Lindblad-type superoperators in Eq. (5) are listed below:

$$\mathcal{L}_H\hat{\rho} = \frac{\gamma_h}{2}[(n_h+1)(2\hat{\sigma}_{g1}\hat{\rho}\hat{\sigma}_{g1}^{\dagger} - \hat{\sigma}_{g1}^{\dagger}\hat{\sigma}_{g1}\hat{\rho} - \hat{\rho}\hat{\sigma}_{g1}^{\dagger}\hat{\sigma}_{g1}) + n_h(2\hat{\sigma}_{g1}^{\dagger}\hat{\rho}\hat{\sigma}_{g1} - \hat{\sigma}_{g1}\hat{\sigma}_{g1}^{\dagger}\hat{\rho} - \hat{\rho}\hat{\sigma}_{g1}\hat{\sigma}_{g1}^{\dagger})], \quad (6)$$

$$\mathcal{L}_{1c}\hat{\rho} = \sum_{i,j=1}^{2}\frac{\gamma_{ijc}}{2}[(n_{1c}+1)(\hat{\sigma}_{j2}\hat{\rho}\hat{\sigma}_{i2}^{\dagger} + \hat{\sigma}_{i2}\hat{\rho}\hat{\sigma}_{j2}^{\dagger} - \hat{\sigma}_{j2}^{\dagger}\hat{\sigma}_{i2}\hat{\rho} - \hat{\rho}\hat{\sigma}_{i2}^{\dagger}\hat{\sigma}_{j2}) + n_{1c}(\hat{\sigma}_{i2}^{\dagger}\hat{\rho}\hat{\sigma}_{j2} + \hat{\sigma}_{j2}^{\dagger}\hat{\rho}\hat{\sigma}_{i2} - \hat{\sigma}_{i2}\hat{\sigma}_{j2}^{\dagger}\hat{\rho} - \hat{\rho}\hat{\sigma}_{j2}\hat{\sigma}_{i2}^{\dagger})], \quad (7)$$

$$\mathcal{L}_{2c}\hat{\rho} = \sum_{i,j=1}^{2}\frac{\Gamma_{ijc}}{2}[(n_{2c}+1)(\hat{\sigma}_{gj}\hat{\rho}\hat{\sigma}_{gi}^{\dagger} + \hat{\sigma}_{gi}\hat{\rho}\hat{\sigma}_{gj}^{\dagger} - \hat{\sigma}_{gj}^{\dagger}\hat{\sigma}_{gi}\hat{\rho} - \hat{\rho}\hat{\sigma}_{gi}^{\dagger}\hat{\sigma}_{gj}) + n_{2c}(\hat{\sigma}_{gi}^{\dagger}\hat{\rho}\hat{\sigma}_{gj} + \hat{\sigma}_{gj}^{\dagger}\hat{\rho}\hat{\sigma}_{gi} - \hat{\sigma}_{gi}\hat{\sigma}_{gj}^{\dagger}\hat{\rho} - \hat{\rho}\hat{\sigma}_{gj}\hat{\sigma}_{gi}^{\dagger})], \quad (8)$$

$$\mathcal{L}_{3c}\hat{\rho} = \frac{\gamma_e}{2}[(n_e+1)(2\hat{\sigma}_{21}\hat{\rho}\hat{\sigma}_{21}^{\dagger} - \hat{\sigma}_{21}^{\dagger}\hat{\sigma}_{21}\hat{\rho} - \hat{\rho}\hat{\sigma}_{21}^{\dagger}\hat{\sigma}_{21}) + n_e(2\hat{\sigma}_{21}^{\dagger}\hat{\rho}\hat{\sigma}_{21} - \hat{\sigma}_{21}\hat{\sigma}_{21}^{\dagger}\hat{\rho} - \hat{\rho}\hat{\sigma}_{21}\hat{\sigma}_{21}^{\dagger})], \quad (9)$$

$$\mathcal{L}_{\Gamma}\hat{\rho} = \sum_{i=1}^{2}\frac{\Gamma_i}{2}(2\hat{\sigma}_{\alpha ii}\hat{\rho}\hat{\sigma}_{\alpha ii} - \hat{\rho}\hat{\sigma}_{\alpha ii} - \hat{\sigma}_{\alpha ii}\hat{\rho}), \quad (10)$$

$$\mathcal{L}_{\chi\Gamma}\hat{\rho} = \sum_{i=1}^{2}\frac{\chi\Gamma_i}{2}(2\hat{\sigma}_{bi}\hat{\rho}\hat{\sigma}_{bi}^{\dagger} - \hat{\rho}\hat{\sigma}_{\alpha ii} - \hat{\sigma}_{\alpha ii}\hat{\rho}). \quad (11)$$

Equation (6) describes the effect of the high temperature reservoirs, where n_h denotes the average photon numbers of the high temperature reservoir, while the low temperature reservoir has the average phonon numbers $n_{1c} = [\exp(\frac{(E_{e_2}-E_{\alpha_i})}{k_B T_a})]^{-1}$ in Eq. (7), $\gamma_{iic} = \gamma_{ic}$ ($\gamma_{jjc} = \gamma_{jc}$) are the spontaneous decay rates from level $|e_2\rangle$ to level $|\alpha_i\rangle$ $(i = 1,2)$ respectively. The cross-coupling γ_{ijc} describes the effect of Fano interference. It is assumed that $\gamma_{ijc} = \gamma_{jic}$ with $\gamma_{ijc} = \eta_1\sqrt{\gamma_{ic}\gamma_{jc}}$ $(i,j = 1,2)$, where η_1 describes the quantum interference intensity with $\eta_1 = 1$ meaning the fully quantum interference and $\eta_1 = 0$ for no interference. Similarly, another low temperature reservoir is described by Eq. (8), with $n_{2c} = [\exp(\frac{(E_{\beta_i}-E_g)}{k_B T_a})]^{-1}$ being the cold reservoir phonon numbers. $\Gamma_{ijc} = \Gamma_{jic}$ is defined by $\Gamma_{ijc} = \eta_2\sqrt{\Gamma_{ic}\Gamma_{jc}}$ in Eq. (8), which describes the Fano interference induced by the spontaneous decay rates, $\Gamma_{iic} = \Gamma_{ic}$ ($\Gamma_{jjc} = \Gamma_{jc}$) $(i,j = 1,2)$ from level $|\beta_{i,(i=1,2)}\rangle$ to level $|g\rangle$ with η_2 denoting the quantum interference robustness. In Eq. (9), $n_e = [\exp(\frac{(E_{e_1}-E_{e_2})}{k_B T_a})]^{-1}$ is the corresponding thermal occupation numbers of the photon functioned by the robust coupled-dipoles J at temperature T_a. $\hat{\sigma}_{\alpha_{ii}} = |\alpha_i\rangle\langle\alpha_i|_{(i=1,2)}$ is defined in Eqs. (10) and (11). Next, we will quantitatively depict the electron transfer mechanisms in the photosynthetic RC via the density matrix dynamic element equations (see Appendix A).

In the present model, we will explore the effect of the coupled-dipoles on the photosynthetic performance evaluated by the population dynamics of the two coupled sites, j–V characteristics, and output power. For the sake of calculation, the output currents through two charge-separation pathways, $|\alpha_1\rangle \to |\beta_1\rangle$ (path 1) and $|\alpha_2\rangle \to |\beta_2\rangle$ (path 2) are set to be the same in the following discussion, i.e., the rates of release $\Gamma_1 = \Gamma_2$. Not only that, the total delivered voltage of the two channels is defined as the sum of their chemical potential differences between state $|\alpha_1\rangle$ ($|\alpha_2\rangle$) and state $|\beta_1\rangle$ ($|\beta_2\rangle$), $eV = \sum_{i=1}^{2}[E_{\alpha_i} - E_{\beta_i} + k_B T_a \ln(\frac{\rho_{\alpha_i\alpha_i}}{\rho_{\beta_i\beta_i}})]$. The selected parameters (shown in Table 1) $E_{\alpha_i}$and E_{β_i} $(i = 1,2)$ through the two charge-separation pathways are referred to Ref. [23] with e being the elementary electron charge. Therefore, the performance of photosynthetic QHE in RC can be numerically evaluated by the current–voltage (j–V) characteristics and the generated power $P = j \cdot V$. The direct impact of the coupled-dipoles on the photosynthetic performance will be described by the population dynamics of the two coupled sites $|e_1\rangle$ and $|e_2\rangle$.

In Fig. 2, the population dynamics of states $|e_1\rangle$ and $|e_2\rangle$ are plotted in Fig. 2(a) and its inset, and the numerical output power, steady-state j–V characteristic versus different robustness of the coupled-dipoles are illustrated in Fig. 2(b) and its inset with $J = 0.001$, 0.005, 0.009, 0.013, 0.017, and 0.021. The quantum interference intensities are set as $\eta_1 = 0.35$ and $\eta_2 = 0.35$ in our numeral simulation. The antipodal influences

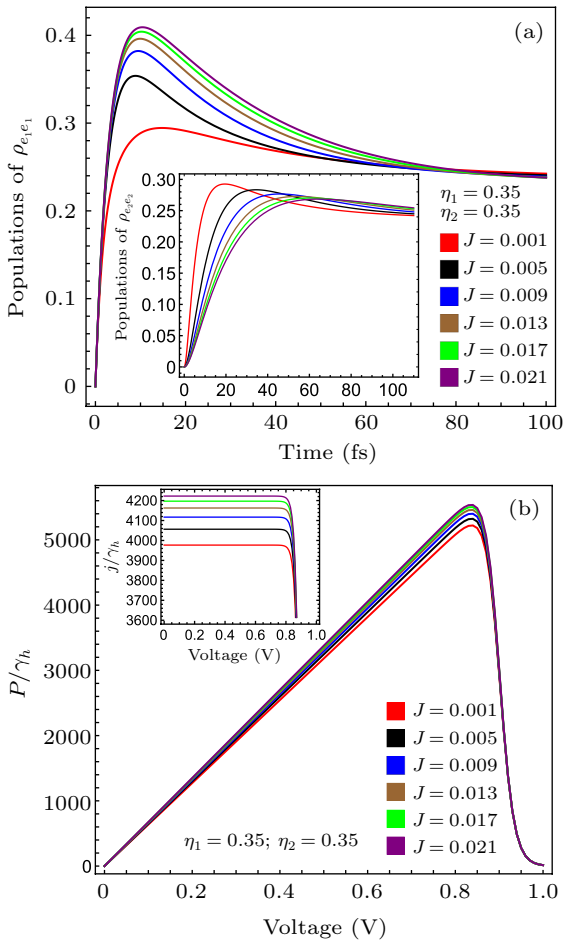


Fig. 2. (a) Population dynamics of level $|e_1\rangle$ and level $|e_2\rangle$, (b) j–V characteristic and power P of this QHE with different $J = 0.001$, 0.005, 0.009, 0.013, 0.017, and 0.021. The quantum interference intensities are selected as $\eta_1 = 0.35$ and $\eta_2 = 0.35$. Other parameters are taken from Table 1.

on the two coupled sites $|e_1\rangle$ and $|e_2\rangle$ are shown by the peak populations in the range of [0, 100 fs] in Fig. 2(a). As for the excited state $|e_1\rangle$, the increasing population is generated by the more robust coupled-dipoles J. However, the peak populations of ρ_{e2e2} decrease with the increase of coupled-dipole interactions J in the same time range, [0, 100 fs] in Fig. 2(a). What's more, it notes that the influence of J on the peak populations in the excited state $|e_1\rangle$ is sensitive, which can be drawn from the peak differences between the purple and red curves with $J = 0.001$ and 0.021, respectively. The results indicate that more excited electrons are transferred to the exciton state $|e_1\rangle$ by the enhanced coupled-dipoles J. The large population differences indicate better photosynthetic performance, which will be manifested by the j–V characteristic curves and output power in Fig. 2(b). From the inset in Fig. 2(b), the curves show that the increasing short-circuit currents and peak powers are achieved by the increase of J. The above results demonstrate the coupled-dipoles between the two different charge separation pathways throw a positive impact on its photosynthetic performance.

In this proposed photosynthetic QHE model, what is the role of the coupled-dipoles between the two charge separation pathways in the Fano interference? Figure 3 demonstrates that the Fano interference caused by the cross-coupling γ_{ijc} is deactivated owing to the coupled-dipoles. In Fig. 3, the population dynamics of states $|e_1\rangle$ and $|e_2\rangle$ are regulated by the Fano interference strength η_1. Counter-intuitively, we notice that the increasing Fano interference η_1 throws almost no influence on the population dynamics of state $|e_2\rangle$, and the zoomed insets of populated $|e_1\rangle$ show minimal influence when the coupled-dipoles J is in the range of $0.001 \leq J \leq 0.035$ (Figs. 3(a)–3(c)), which is a similar result mentioned by the previous work.[25] When the coupled-dipoles J is in the range of $0.035 \leq J \leq 0.24$, and now η_1 plays a more prominent role after 60 fs (cf. the solid lines with different $\eta_1 = 0$, 0.3, 0.6, 0.9), although its impact on their peaks of the population of level $|e_1\rangle$ is not significant.

Table 1. Model parameters used in the numerical calculations.

	Values	Units
$E_{D_1} - E_g = E_{D_2} - E_g$	1.8	eV
$E_{D_1} - E_{\alpha_1} = E_{D_1} - E_{\alpha_2}$	0.2	eV
$E_{\beta_1} - E_g = E_{\beta_2} - E_g$	0.2	eV
γ_h	2.48×10^{-6}	eV
γ_e	0.025	eV
$\gamma_{1c} = \gamma_{2c}$	0.012	eV
$\Gamma_1 = \Gamma_2$	0.124	eV
$\Gamma_{1c} = \Gamma_{2c}$	0.0248	eV
n_h	6000	
T_a	300	
χ	0.2	

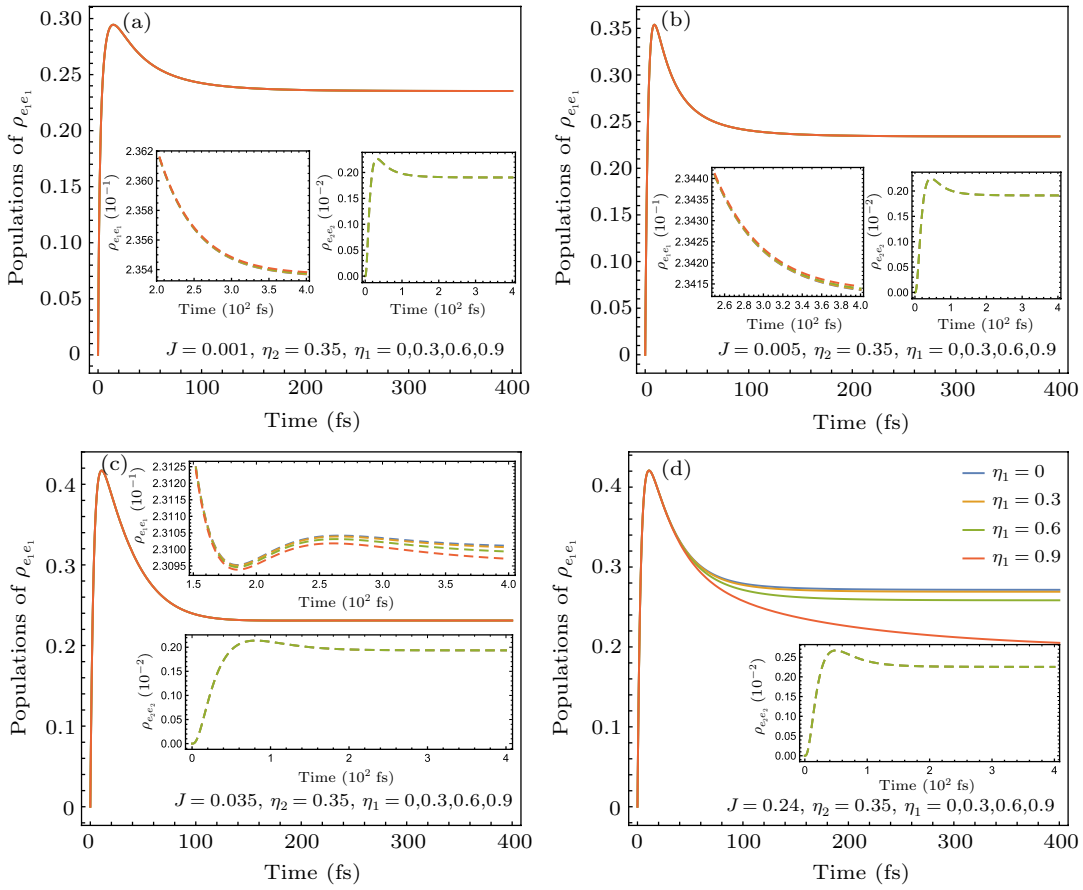


Fig. 3. (a)–(d) Population dynamics of levels $|e_1\rangle$ and $|e_2\rangle$ under different quantum interference intensities $\eta_1 = 0$, 0.3, 0.6, 0.9, and $\eta_2 = 0.35$ with different coupled-dipoles robustness $J = 0.001$, 0.005, 0.035, and 0.24, respectively. Other parameters are the same as those in Fig. 2.

Some previous work[40] mentioned that certain "dark" states could be generated by the dipole-dipole interactions in a photosynthetic process. Maybe we can take some cues for the physical phenomenon in this proposed model, and we speculate that the coupled-dipoles between the two charge separation pathways may also produce a dark state, which disables one chlorophyll located at the center of the PSII RC, forming one exciton state $|e_1\rangle$ being the primary electron donor. Thus, the Fano interference caused by the cross-coupling γ_{ijc} is deactivated. Changing the parameter η_1 has no substantial influence on the population dynamics of state $|e_2\rangle$. But more electrons are transferred to the exciton state $|e_1\rangle$, which ultimately results in the increasing peak population on the exciton state $|e_1\rangle$.

In this photosynthetic QHE system, the influence of J on another quantum interference originating from the crossing spontaneous decay rates, Γ_{1c} and Γ_{2c} from level $|\beta_{i,(i=1,2)}\rangle$ to level $|g\rangle$ stimulates our curiousness. Therefore, we similarly focus on the influence involving the robustness of J on the quantum interference described by η_2. It notes that the inactive short-lived quantum interference η_2 still appears in the range of $[0, 100$ fs$]$. With the time evolution, the influence of η_2 gradually works on the population dynamics of levels $|e_1\rangle$ and $|e_2\rangle$ in the subsequent time range shown in Figs. 4(a) and 4(b). We also notice that the increasing robustness of J brings about an increase in the population difference between $|e_1\rangle$ and $|e_2\rangle$, which will indicate an enhancement of photosynthetic performance in this QHE model. The j–V characteristic and power P in Figs. 4(c) and 4(d) demonstrate this prediction. Curves in Figs. 4(c) and 4(d) with the same color signify the identical quantum interference η_2. It notes that the j–V characteristic and power P increase with the coupled-dipoles robustness J but decrease with η_2. And the change from the dashed to solid lines with the same color manifests the enhanced photosynthetic performance due to the increasing coupled-dipoles robustness J. In this photosynthetic QHE system, the increasing η_2 indicates more electrons transition to the state $|g\rangle$, which results in the decreasing j–V characteristic and power P in Figs. 4(c) and 4(d). The curves with the same color illustrate that the negative function of quantum interference η_2 can be suppressed by the coupled-dipoles robustness J. Finally, we would like to point out that these conclusions are drawn from a typical photosynthetic RC model, and it may have universal theoretical significance for the design of artificial photosynthetic devices.

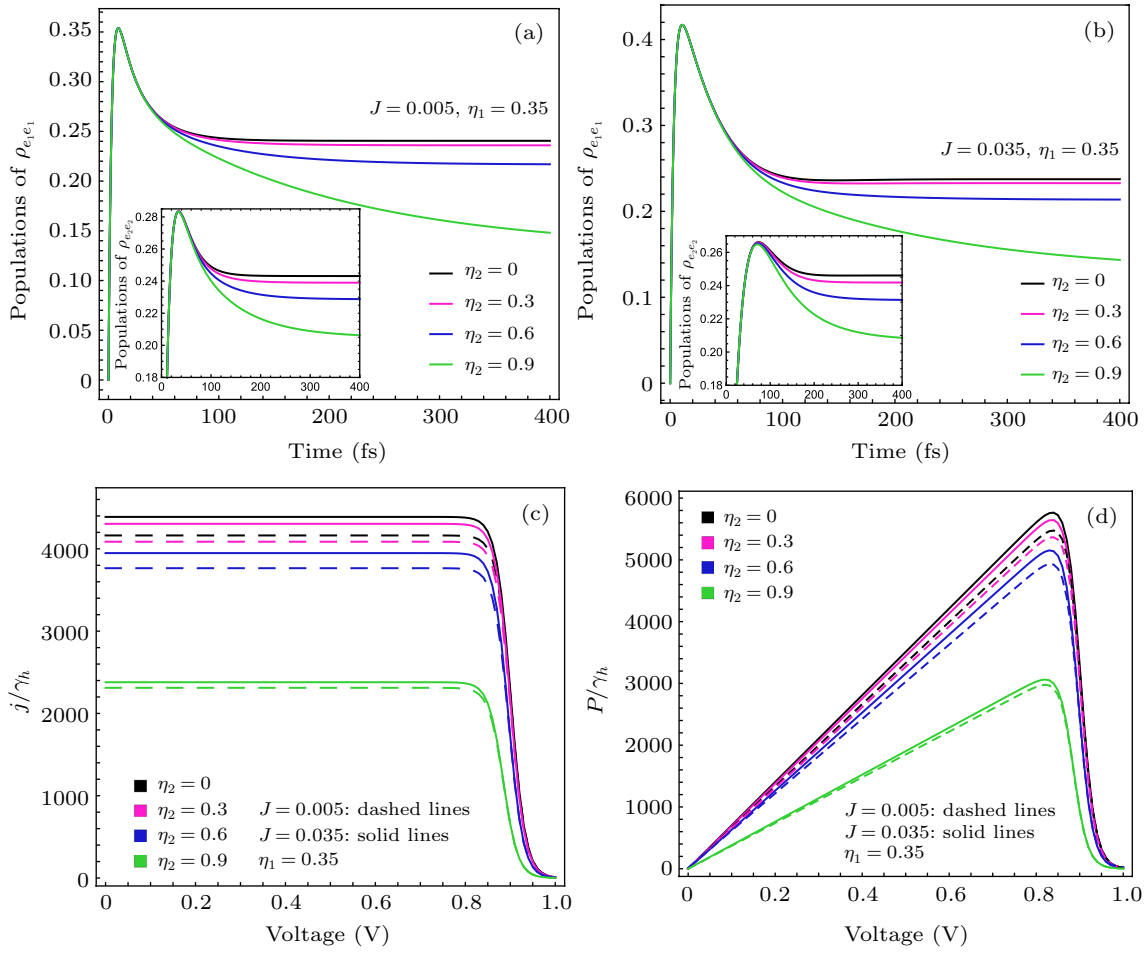


Fig. 4. Population dynamics of levels $|e_1\rangle$ and $|e_2\rangle$ in (a) and (b), and j–V characteristic and power P in (c) and (d) with different quantum interference intensities $\eta_2 = 0$, 0.3, 0.6, 0.9, and $\eta_1 = 0.35$ under different robustness of the coupled-dipoles $J = 0.005$ and $J = 0.035$. Other parameters are the same as those in Fig. 2.

3. Conclusion

In this proposed photosynthetic QHE model, the roles of the coupled-dipoles between two-charge separation pathways were quantitatively explored in the photosynthetic performance. The results evaluated by the population dynamics, j–V characteristics, and power P demonstrate that the photosynthetic performance is greatly enhanced but quantum interference is deactivated by the coupled-dipoles, i.e., the increasing J makes η_1 have minimal effect on the populated $|e_1\rangle$ but no effect on the populated $|e_2\rangle$ which brings out more electrons transfer to the exciton state $|e_1\rangle$ and ultimately results in the increasing peak population on the exciton state $|e_1\rangle$. However, the increasing J is beneficial to the enhancement of the photovoltaic performance evaluated by j–V characteristic and power P, although the increasing J makes η_2 have a negative impact. We argue that it is a new operating regime of the coupled-dipoles between two-charge separation pathways in the energy transport process in the biological photosynthetic, and some artificial strategies may be motivated by this photosynthetic QHE model.

Appendix A

The density matrix dynamic element equations are given as follows:

$$
\begin{aligned}
\dot{\rho}_{e_1e_1} &= -\gamma_e[(n_e+1)\rho_{e_1e_1} - n_e\rho_{e_2e_2}] \\
&\quad -\gamma_h[(n_h+1)\rho_{e_1e_1} - n_h\rho_{\rm gg}], \\
\dot{\rho}_{e_2e_2} &= \gamma_e[(n_e+1)\rho_{e_1e_1} - n_e\rho_{e_2e_2}] \\
&\quad -\gamma_{1c}[(n_{1c}+1)\rho_{e_2e_2} - n_{c1}\rho_{\alpha_1\alpha_1}] \\
&\quad -\gamma_{2c}[(n_{1c}+1)\rho_{e_2e_2} - n_{1c}\rho_{\alpha_2\alpha_2}] \\
&\quad +2\gamma_{12c}n_{c1}Re[\rho_{\alpha_1\alpha_2}], \\
\dot{\rho}_{\alpha_1\alpha_1} &= \gamma_{1c}[(n_{1c}+1)\rho_{e_2e_2} - n_{1c}\rho_{\alpha_1\alpha_1}] - \gamma_{12c}n_{1c}Re[\rho_{\alpha_1\alpha_2}] \\
&\quad -(1+\lambda)\Gamma_1\rho_{\alpha_1\alpha_1}, \\
\dot{\rho}_{\alpha_2\alpha_2} &= \gamma_{1c}[(n_{1c}+1)\rho_{e_2e_2} - n_{1c}\rho_{\alpha_1\alpha_1}] - \gamma_{12c}n_{1c}Re[\rho_{\alpha_1\alpha_2}] \\
&\quad -(1+\lambda)\Gamma_2\rho_{\alpha_2\alpha_2}, \\
\dot{\rho}_{\alpha_1\alpha_2} &= -{\rm i}\Delta_1\rho_{\alpha_1\alpha_2} - \frac{1}{2}(\gamma_{1c}+\gamma_{2c})n_{1c}\rho_{\alpha_1\alpha_2} \\
&\quad +\frac{1}{2}\gamma_{12c}[2(n_{1c}+1)\rho_{e_2e_2} - n_{1c}\rho_{\alpha_2\alpha_2} - n_{1c}\rho_{\alpha_1\alpha_1}], \\
\dot{\rho}_{\beta_1\beta_1} &= \Gamma_1\rho_{\alpha_1\alpha_1} - \Gamma_{1c}[(n_{2c}+1)\rho_{\beta_1\beta_1} - n_{2c}\rho_{\rm gg}] \\
&\quad -\Gamma_{12c}(n_{2c}+1)Re[\rho_{\beta_1\beta_2}], \\
\dot{\rho}_{\beta_2\beta_2} &= \Gamma_2\rho_{\alpha_2\alpha_2}\Gamma_{2c}[(n_{2c}+1)\rho_{\beta_2\beta_2} - n_{2c}\rho_{\rm gg}] \\
&\quad -\Gamma_{12c}(n_{2c}+1){\rm Re}[\rho_{\beta_1\beta_2}], \\
\dot{\rho}_{\beta_1\beta_2} &= -{\rm i}\Delta_2\rho_{\beta_1\beta_2} - \frac{1}{2}(\Gamma_{1c}+\Gamma_{2c})(n_{2c}+1)\rho_{\beta_1\beta_2} \\
&\quad -\frac{1}{2}\Gamma_{12c}[(n_{2c}+1)\rho_{\beta_1\beta_1} + (n_{2c}+1)\rho_{\beta_2\beta_2} - 2n_{2c}\rho_{\rm gg}], \\
\rho_{\rm gg} &= 1-\rho_{e_1e_1}-\rho_{e_2e_2}-\rho_{\alpha_1\alpha_1}-\rho_{\alpha_2\alpha_2}-\rho_{\beta_1\beta_1}-\rho_{\beta_2\beta_2}, \qquad \text{(A1)}
\end{aligned}
$$

where $\Delta_1 = E_{\alpha_1} - E_{\alpha_2}$ and $\Delta_2 = E_{\beta_1} - E_{\beta_2}$ are the splitting of the states $|\alpha_1\rangle$ ($|\alpha_2\rangle$) and $|\beta_1\rangle$ ($|\beta_2\rangle$). We utilize the equations to simulate the dynamics of the reaction center.

References

[1] Engel G S, Calhoun T R, Read E L, Ahn T K, Mancal T, Cheng Y C, Blankenship R E and Fleming G R 2007 *Nature* **446** 782
[2] Akihito L and Fleming G R 2009 *Proc. Natl. Acad. Sci. USA* **106** 17255
[3] Zhu J, Kais S, Rebentrost P and Aspuru-Guzik A 2011 *J. Phys. Chem. B* **115** 1531
[4] Caram J R, Lewis N H C, Fidler A F and Engel G S 2012 *J. Chem. Phys.* **136** 17255
[5] Rebentrost P, Mohseni M, Kassal I, Lloyd S and Aspuru-Guzik A 2009 *New J. Phys.* **11** 033003
[6] Killoran N, Huelga S F and Plenio M B 2015 *J. Chem. Phys.* **143** 155102
[7] Mohseni M, Rebentrost P, Lloyd S and Aspuru-Guzik A 2008 *J. Chem. Phys.* **129** 174106
[8] Esták Z and Blankenship R E 2002 *Photosynthetica* **40** 12
[9] Gilmore J and McKenzie R H 2008 *J. Phys. Chem. A* **112** 2162
[10] Caruso F, Chin A W, Datta A, Huelga S F and Plenio M B 2009 *J. Chem. Phys.* **131** 105106
[11] Chen H B, Chiu P Y and Chen Y N 2016 *Phys. Rev. E* **94** 052101
[12] Collini E, Wong C Y, Wilk K E, Curmi P M G, Brumer P and Scholes G D 2010 *Nature* **463** 644
[13] Romero E, Augulis R, Novoderezhkin V I, Ferretti M O, Thieme J, Zigmantas D and Grondelle R V 2014 *Nat. Phys.* **10** 676
[14] Zhao S C and Chen J Y 2019 *New J. Phys.* **21** 103015
[15] Fingerhut B P, Zinth W and Vivie-Riedle R de 2010 *Phys. Chem. Chem. Phys.* **12** 422
[16] Chen J Y and Zhao S C 2020 *Chin. Phys. B* **29** 064207
[17] Blankenship R E, Tiede D M, Barber J, Brudvig G W, Fleming G, Ghirardi M, Gunner M, Junge W, Kramer D M, Melis A, Moore T A, Moser C, Nocera D G, Nozik A J, Ort D R, Parson W W, Prince R C and Sayre R T 2011 *Science* **332** 805
[18] Zhao S C, Chen J Y and Li X 2020 *Eur. Phys. J. Plus* **135** 892
[19] Fleming G R 2009 *Proc. Natl. Acad. Sci. USA* **106** 17255
[20] Huelga S F and Plenio M B 2013 *Contemp. Phys.* **54** 181
[21] Zong X L, Song W, Zhou J, Yang M, Yu L B and Cao Z L 2018 *Quantum Inf. Process* **17** 158
[22] Dorfman K E, Voronine D V, Mukamel S and Scully M O 2013 *Proc. Natl. Acad. Sci. USA* **110** 2746
[23] Creatore C, Parker M A, Emmott S and Chin A W 2013 *Phys. Rev. Lett.* **111** 253601
[24] Su S H, Luo X Q, Chen J C and Sun C P 2016 *Europhys. Lett.* **115** 30002
[25] Qin M, Shen H Z and Yi X X 2016 *J. Chem. Phys.* **44** 125103
[26] Panitchayangkoon G, Hayes D, Fransted K A, Caram J R, Harel E, Wen J, Blankenship R E and Engel G S 2010 *Proc. Natl. Acad. Sci. USA* **107** 12766
[27] Collini E, Wong C Y, Wilk K E, Curmi P M G, Brumer P and Scholes G D 2010 *Nature* **463** 644
[28] Huo P and Coker D F 2010 *J. Chem. Phys.* **133** 184108
[29] Christensson N, Kauffmann H F, Pullerits T and Manal T 2012 *J. Phys. Chem. B* **116** 7449
[30] Cardona A, Sedoud T, Cox N and William R A 2012 *Biochim. Biophys. Acta-Bioenergetics* **1817** 26
[31] Arp T B, Barlas Y, Aji V and Gabor N M 2015 *Nano Lett.* **16** 7461
[32] Qin M, Shen H Z, Zhao X L and Yi X X 2017 *Phys. Rev. A* **96** 012125
[33] Leonardo A P and Paul B 2011 *J. Phys. Chem. Lett.* **2** 2728
[34] Novoderezhkin V I, Dekker J P and Grondelle R Van 2007 *Biophys. J.* **93** 1293
[35] Elisabet R V, Stokkum I H M, Novoderezhkin V I, Dekker J P and Grondelle R V 2010 *Biochemistry* **49** 4300
[36] Novoderezhkin V I, Romero E, Dekker J P and Grondelle R V 2015 *ChemPhysChem* **12** 681
[37] Chen J Y and Zhao S C 2020 *Eur. Phys. J. Plus* **135** 1
[38] Chen H B, Lien J Y, Hwang C C and Chen Y N 2014 *Phys. Rev. E* **89** 42147
[39] Zhao S C and Wu Q X 2020 *Superlattices and Microstructures* **137** 106329
[40] Zhang Y T, Oh S, Alharbi F H, Engel G S and Kais S 2015 *Phys. Chem. Chem. Phys.* **17** 5743